Original Article

Preclinical *in vivo* longitudinal assessment of KG207-M as a disease-modifying Alzheimer's disease therapeutic

Min Su Kang[1,2,3] (iD), Monica Shin[1,2], Julie Ottoy[1] (iD),
Arturo Aliaga Aliaga[1,2,3], Sulantha Mathotaarachchi[1,2],
Kely Quispialaya[1], Tharick A Pascoal[1,2], D Louis Collins[3],
M. Mallar Chakravarty[2], Axel Mathieu[2], Åsa Sandelius[4],
Kaj Blennow[4,5], Henrik Zetterberg[4,5,6,7], Gassan Massarweh[3],
Jean-Paul Soucy[3], A Claudio Cuello[8], Serge Gauthier[1,2,3],
Michael Waterston[9], Nathan Yoganathan[10], Etienne Lessard[11],
Arsalan Haqqani[11], Kerry Rennie[11], Danica Stanimirovic[11],
Balu Chakravarthy[11] and Pedro Rosa-Neto[1,2,3] (iD)

Abstract

In vivo biomarker abnormalities provide measures to monitor therapeutic interventions targeting amyloid-β pathology as well as its effects on downstream processes associated with Alzheimer's disease pathophysiology. Here, we applied an *in vivo* longitudinal study design combined with imaging and cerebrospinal fluid biomarkers, mirroring those used in human clinical trials to assess the efficacy of a novel brain-penetrating anti-amyloid fusion protein treatment in the McGill-R-Thy1-APP transgenic rat model. The bi-functional fusion protein consisted of a blood-brain barrier crossing single domain antibody (FC5) fused to an amyloid-β oligomer-binding peptide (ABP) via Fc fragment of mouse IgG (FC5-mFc2a-ABP). A five-week treatment with FC5-mFc2a-ABP (loading dose of 30 mg/Kg/iv followed by 15 mg/Kg/week/iv for four weeks) substantially reduced brain amyloid-β levels as measured by positron emission tomography and increased the cerebrospinal fluid amyloid-$\beta_{42/40}$ ratio. In addition, the 5-week treatment rectified the cerebrospinal fluid neurofilament light chain concentrations, resting-state functional connectivity, and hippocampal atrophy measured using magnetic resonance imaging. Finally, FC5-mFc2a-ABP (referred to as KG207-M) treatment did not induce amyloid-related imaging abnormalities such as micro-hemorrhage. Together, this study demonstrates the translational values of the designed preclinical studies for the assessment of novel therapies based on the clinical biomarkers providing tangible metrics for designing early-stage clinical trials.

Keywords

[1]Translational Neuroimaging Laboratory, McGill University Research Centre for Studying in Aging, Montreal, QC, Canada
[2]Douglas Mental Health University Institute, Montreal, Canada
[3]McConnell Brain Imaging Centre, McGill University, Montreal, QC, Canada
[4]Department of Psychiatry and Neurochemistry, the Sahlgrenska Academy at the University of Gothenburg, Mölndal, Sweden
[5]Clinical Neurochemistry Laboratory, Sahlgrenska University Hospital, Mölndal, Sweden
[6]UK Dementia Research Institute at UCL, London, UK
[7]Department of Molecular Neuroscience, UCL Institute of Neurology, London, UK

[8]Department of Pharmacology and Therapeutics, McGill University, Montreal, QC, Canada
[9]Centre for Imaging Technology Commercialization, London, ON, Canada
[10]KalGene Pharmaceuticals Inc., Montreal, Canada
[11]Human Health Therapeutics, National Research Council of Canada, Ottawa, ON, Canada

Corresponding author:
Pedro Rosa-Neto, Translational Neuroimaging Laboratory, McGill University Research Center for Studies in Aging, Douglas Mental Health Institute, McGill University, 6825 LaSalle Blvd, Montreal, QC H4H1R3, Canada.
Email: pedro.rosa@mcgill.ca

Introduction

Amyloid-β (Aβ) aggregates remain an attractive therapeutic target for Alzheimer's disease (AD) based on a multitude of genetic and cellular evidence supporting the central role of Aβ in AD pathophysiology.[1–5] Consequently, there have been great efforts to develop therapeutics that target Aβ and its clearance. One approach has been immunotherapy with anti-amyloid antibodies.[6–8] Despite promising preclinical studies demonstrating Central Nervous System (CNS) Aβ clearance and improvement in cognitive deficits in transgenic mice, several anti-amyloid immunotherapies have failed in clinical trials.[6,7] Possible reasons for this lack of clinical translation include their low blood-brain barrier (BBB) penetrance, failure to target the appropriate Aβ species, or safety concerns, such as amyloid-related imaging abnormalities (ARIA).[9–11] To address these concerns at the preclinical level, we have recently developed a biomarker platform that allows longitudinal assessments of the effects of an anti-amyloid therapy on imaging and cerebrospinal fluid (CSF) biomarkers using the APP transgenic rat model. The platform provides measures of Aβ load obtained with [^{18}F]AZD4694 positron emission tomography (PET) and CSF A$\beta_{42/40}$ ratio.[12,13] In addition, this platform provides measures of neuronal injury via CSF neurofilament light chain (NFL), structural changes using T1 weighted MRI (sMRI), and brain connectivity estimated by resting-state functional MRI (rs-fMRI). Also, potential brain microhemorrhages (ARIA-H) are detected using susceptibility MRI. By providing the same metrics utilized in human clinical trials, this platform increases the likelihood of translation of assessed target engagement and therapeutic efficacy from preclinical studies to early-stage clinical trials in humans.

This *in vivo* longitudinal imaging and CSF biomarker platform allowed us to evaluate the effects of a novel biopharmaceutical construct, FC5-mFc-ABP (amyloid binding protein), on Aβ clearance, downstream effects on the neuronal injury, and disease-modifying response using a repeated dosing prospective strategy. FC5-mFc2a-ABP is a bi-functional fusion protein consisting of the BBB-crossing camelid single-domain antibody FC5[14] fused to the N-terminus of Fc fragment of mouse IgG2a, and amyloid binding peptide (ABP) fused to the C-terminus of Fc. Previous *in vitro* and *ex vivo* studies have shown that ABP selectively binds to Aβ_{42} oligomers and Aβ deposits in the brains of AD transgenic mice and post-mortem human brains from AD patients, respectively.[15,16] We have successfully fused ABP with FC5 via mFc and expressed the fusion protein in CHO cells. In this study, we have evaluated the *in vivo* target engagement and efficacy of FC5-mFc2a-ABP (referred to as KG207-M henceforth) using a rat model of AD-like Aβ pathology carrying hAPP with Swedish and Indiana mutations called McGill-R-Thy1-APP (Tg).[2] This model allows longitudinal biomarker assessments based on imaging and biochemical methods that are translational in nature. Here, we hypothesized that KG207-M would be transported across the BBB and show target engagement by Aβ clearance, achieving therapeutic benefit. We report successful target engagement by demonstrating reduced Aβ load, rectifying Aβ-induced neuronal injury, functional improvements, and safety (no evidence of ARIA-H) after a 5-week treatment.

Materials and methods

Study design

This study was designed to characterize BBB penetrance, target engagement, and safety related to ARIA-H following five weeks of anti-amyloid treatment in the Aβ Tg rat model (Figure 1). This is the first *in vivo* study to investigate the direct effect size and power of the KG207-M treatment in the BBB penetrance, target engagement, and ARIA-H in rats. Therefore, we calculated our power analysis based on the effect size (dz = 3.21) of Aβ pathology progression in the McGill-R-Thy1-APP rat model from our previous cohort data. To be able to observe the Aβ pathology progression at α error = 0.05 and power $(1-\beta) = 0.95$ given the effect size of normal progression, we would need four animals. This led to including four animals in the control to reflect the natural progression, while the remaining animals were included to increase the power to capture the effects of the BBB penetrance, target engagement, and safety profile. Here, our Tg cohort started with a total of 17 animals where they underwent CSF collection from 10–19 months. However, four animals were sacrificed at 13.7, 17.4, and 18 months of age due to testicular tumours before the therapeutic intervention began. Consequently, the control group (Tg-SAL) included four (two males and two females) and the treatment group (Tg-ABP) included the remaining nine animals (six males and three females) randomly selected while matching for the sex and body weight. To note, we have matched the sex rather than stratifying as a group as the effect of sex/gender will be investigated in subsequent studies. However, one Tg-SAL animal died at 23 months of age. Tg-SAL and Tg-ABP groups underwent baseline procedures including PET [^{18}F] AZD4694, sMRI, and rs-fMRI at 21 months and follow-up at 24 months of age. We added susceptibility MRI to assess ARIA-H following the treatment in the follow-up time point. To be able to characterize the
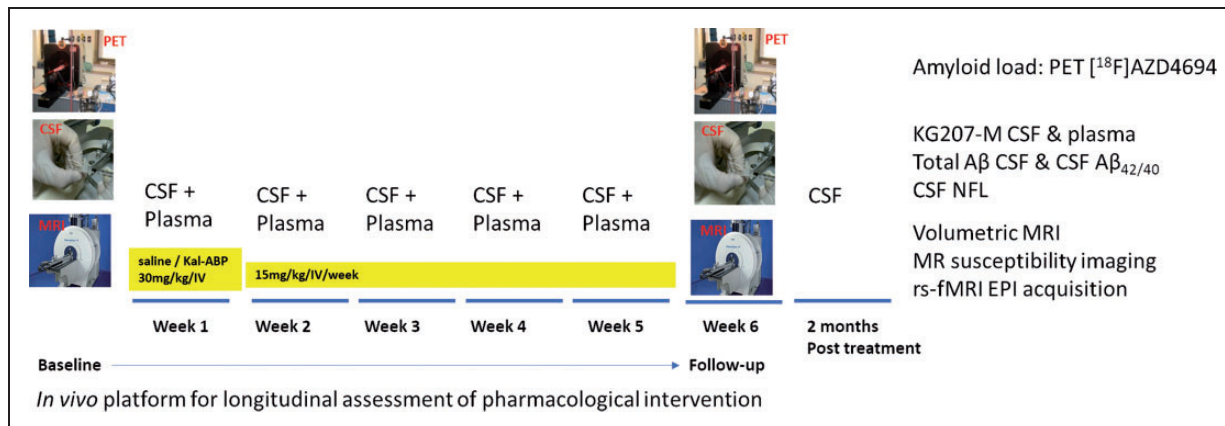
Figure 1. Baseline measurements including PET [^{18}F]AZD4694, sMRI, and rs-fMRI were acquired at 21 months of age. Then, weekly KG207-M injection via tail vein from 22.5-23.5 months (30 mg/Kg/iv initial dose following 15 mg/Kg/iv dose) was followed by a serial CSF collection at the indicated times via cisterna magna after fixing the animals in a stereotaxic apparatus with isoflurane anesthesia. Then, serial blood was collected at the indicated times via the subclavian vein and separated into the plasma via centrifuge. On Week 6 at 24 months old, the follow-up measurements were acquired including PET [^{18}F]AZD4694, sMRI, rs-fMRI, susceptibility MRI, and CSF.

natural progression of the Aβ pathology via PET from the pre-plaque stage, we included additional eight Tg animals from our previous cohort study that underwent the same PET [^{18}F]AZD4694 procedure at 10 and 17 months, effectively increasing the power of the data.[17] Therefore, we characterized the population-based Aβ pathology progression ([^{18}F]AZD4694 PET BP$_{ND}$) from 10, 17, 21, and 24 months in the McGill-R-Thy1-APP rat model. All [^{18}F]AZD4694 images were processed and analyzed in the same methods described below. During the treatment, all animals were subjected to a serial collection of CSF and plasma to characterize the pharmacokinetics. Two months following the study completion, extra CSF samples were collected (at 25 and 26 months) to assess the post-treatment effect. From 744 CSF samples, 139 (18.7%) samples were excluded due to blood contamination. Moreover, two animals (one from Tg-SAL and Tg-ABP) were excluded from the analyses as they had a relatively lower level of Aβ expression with only intraneuronal Aβ hinting as a hemizygous animal.[2] For CSF NFL analysis, only the animals who had undergone the entire experimental protocol without any type of tissue abnormality (abscess or tumour) were included. However, all animals were included in the ARIA-H analysis, including the hemizygous animals. All the animal handling and procedures were blinded to the group identification.

Animals

All procedures described here were performed in compliance with ethics protocols approved by McGill Animal Care Ethics Committee and following the Canadian Council on Animal Care guidelines. All rats were housed at the Douglas Mental Health University Institute animal facility on a 12/12 hr light/darkness cycle with *ad libidum* access to food and water. A starting sample of 17 homozygous McGill-R-Thy1-APP rats on Wistar background was used for the study.

KG207-M and Aβ_{total} quantification using selected reaction monitoring (SRM) in CSF and plasma

FC5-mFc-ABP (KG207-M) fusion protein and Aβ levels in the plasma and CSF were quantified using targeted multiplexed mass spectrometry in selected reaction monitoring mode (SRM) on nanoAcquity UPLC (Waters, Milford, MA) coupled to ESI LTQ XL ETD mass spectrometer (ThermoFisher, Waltham, MA) as previously described.[18] A detailed description can be found in Supplemental Materials.

PET imaging acquisition

All PET images were acquired at 10, 17, 21, and 24 months using CTI Concorde R4 microPET for small animals with [^{18}F]AZD4694 for Aβ load. All rats were under 1.5% isoflurane anesthesia during the scan after the 5% anesthesia induction. The [^{57}Co] rotating point source was used for a 9-minute transmission scan, which was followed by a simultaneous bolus tail vein injection of the radiotracer (Mean injected dose $\pm$ standard deviation at 10 and 17 months in Tg $= 13.3\ 21 \pm 0.9$ MBq; at 21 and 24 months in Tg-SAL $= 10.75 \pm 3.74$ MBq and Tg-ABP $= 10.72 \pm 4.75$ MBq) with a 60-minute emission scan. The image was reconstructed using Maximum A Prior (MAP) algorithm with 27 sequential frames (8×30 s, 6×1 min, 5×2 min,

$8 \times 5\,min$), scatter, dead time, and attenuation corrections.

MRI imaging acquisition

All MRI images were acquired using Bruker 7 T BioSpec 70/30 USR dedicated for small animals. All rats were under 1.5% isoflurane anesthesia during the scan after the 5% anesthesia induction.

All structural images were obtained at 10, 17, 21, and 24 months from Bruker standard 3D-True Fast Imaging with Steady State Precession pulse sequence (FISP). A root-mean-square image with the acquisition in eight phases was performed. Each angle acquisition was acquired in FOV of 36 mm × 36 mm × 36 mm with a matrix of 180 × 180 × 180× of TE/TR of 2.5/5.0 ms with two flip angles of 30° and 2 NEX. The final image was an average of 16 acquisitions with 250 µm isotropic resolution from 46 minutes scan. rs-fMRI images were acquired immediately after the structural scan at 21 and 24 months using the standard Bruker 2D-Spin Echo Planer pulse sequence (2D-SE-EPI). The FOV 25.6 mm × 25.6 mm following rostrocaudal axis with a matrix 64 × 64 at 32 slices of 1.0 mm leading to final resolution 400 µm × 400 µm × 1000 µm and 1.0 mm interslice space was acquired. TE/TR was 15/2000 ms with a flip angle of 70° and 450 repetitions for a total 15 minutes scan resulting in three separate runs.

Susceptibility images were acquired at 24 months with Fast Low Angle Shot (FLASH) sequence with TE/TR of 13/100 ms with 1 NEX at pulse angle 40° in FOV 33.6 mm × 20.81 mm × 14.4 mm with a matrix 208 mm × 72 mm × 335 mm resulting in a final resolution of 0.1 mm × 0.2 mm × 0.1 mm.

PET&MRI imaging processes and analysis

All images were processed using MINC toolkits (www.bic.mni.mcgill.ca/ServicesSoftware) following the pipeline described previously.[17] In brief, all PET images received ridged body transformation to the individual anatomical MRI, which then received affine and nonlinear transformations into sample average template space.[19] Then, [18F]AZD4694 Binding Potential (BP_{ND}) parametric maps were generated using the Simplified Reference Tissue Method (SRTM) and Logan reference method with the cerebellar grey matter as a reference region. The parametric maps were blurred using a 1 mm Full-With Half-Maximum (FWHM) Gaussian kernel. Since both measurements showed congruent results, we have selected to include the SRTM data following our previous publication as this study included the previous cohort data.[17]

Hippocampal volume was acquired based on manual segmentation including hippocampal subiculum, dentate gyri, CA1, CA2, and CA3 according to a rat brain atlas (Paxinos and Watson 6th edition, 2007). The manual segmentation was done before and after the KG207-M treatment at 21 months and 24 months in the individual MRI.

For rs-fMRI, we used AFNI (www.afni.nimh.nih.gov/afni/) for preprocessing where the dynamic functional images were corrected for motion and slice-time corrections, bandpass filtered between 0.01-0.1 Hz, and disregarded the first five frames for possible transient drift. Using anatomical-based cingulate cortex seed from our previous study, a seed-based connectivity map was generated based on FMRISTAT tools (www.math.mcgill.ca/keith/fmristat/) in each run. Then, the individual connectivity maps were transformed via affine and nonlinear transformation into sample average template space and a 1.4 mm FWHM Gaussian blurring kernel was applied. Total three separate runs per subject were combined into each subject connectivity map based on FMRISTAT tools, which produced connectivity effect size, standard deviation and t statistics maps. Then, each subject connectivity map was transformed into z distribution (z-map) by dividing the effect size by standard deviation maps.

Susceptibility MRI was first visually assessed. Then, the susceptibility contrast signals were segmented to represent the possible microhemorrhages. These images received the affine and nonlinear transformation to the template space to acquire the total volume of the susceptibility contrast signal.

CSF collection and analysis

All animals were induced with 5% isoflurane anesthesia for 5–8 minutes and placed in a stereotaxic apparatus. The CSF samples (100–150 µL) were collected via a direct puncture through cisterna magna at 10–26 months old.

Simoa CSF NFL measurements. Rat CSF NFL concentration was determined using the in-house Simoa NFL assay, which has been described in detail previously,[20] with some modifications. Briefly, samples were diluted 100x with assay diluent and incubated for 35 minutes with paramagnetic carboxylated beads (Quanterix Corp, Boston, MA, USA) coated with a mouse anti-neurofilament light antibody (UD1, UmanDiagnostics, Umeå, Sweden) and a biotinylated mouse anti-neurofilament light antibody (UD2, UmanDiagnostics) in a Simoa HD-1 instrument (Quanterix). The bead-conjugated immunocomplex was thoroughly washed before incubation with streptavidin-conjugated β-galactosidase (Quanterix). Thereafter, the bead complex was washed and resorufin β-D-galactopyranoside (Quanterix) was added. The immunocomplex was applied to a multi-well array designed to enable imaging of every single

bead. The average number of enzymes per bead (AEB) of samples was interpolated onto the calibrator curve constructed by AEB measurements on bovine NFL (UmanDiagnostics) serially diluted in assay diluent. Samples were analyzed 'blind' and in duplicate using one batch of reagents. The average repeatability coefficient of variation of a sample with the mean concentration of 18102 pg/mL was 8.5% and intermediate precision was 8.8%, and for a sample with a mean concentration of 9460 pg/mL, repeatability was 8.1% and intermediate precision was 11.5%. All samples analyzed were above the lower limit of quantification (LLOQ).

Simoa CSF Aβ_{42} and Aβ_{40} measurements. Rat CSF concentrations of Aβ_{42} and Aβ_{40} were measured using Quanterix kits according to kit instructions (Simoa Aβ_{42} 2.0 211 and Simoa Aβ_{40} 2.0 218, Quanterix) with a CSF dilution of 100x using the provided assay diluents. For Aβ_{42} CSF measurements, the average repeatability coefficient of variation of a sample with a mean concentration of 1650 pg/mL was 3.2% and intermediate precision was 9.2%, and for a sample with a mean concentration of 641 pg/mL, repeatability was 10.9% and intermediate precision was 16.6%. For Aβ_{40} CSF measurements, repeatability for a sample with a concentration of 5160 pg/mL was 17.2%, and intermediate precision 17.2%, and for a sample with a concentration of 3975 pg/mL repeatability and intermediate precision was 7.3% and 11.8%, respectively. All samples analyzed were above the LLOQ.

Histology

All animals were sacrificed 2 months after the KG207-M treatment and follow-up procedures. They were anesthetized with urethane (1 g/Kg) and perfused transcardially with heparinized phosphate-buffered saline (PBS). Their brains were then collected and immersion-fixed in 4% paraformaldehyde (PFA) for 24 hours. Then, the tissues were washed with PBS three times and fixed in sucrose 30% for 48 hours and transferred to the cryoprotectant (30% sucrose and 30% ethylene glycol) to be stored at $-20°C$. The brains were sectioned at 40 μm in the coronal plane with 480 μ intervals throughout the brain using MultiBrain Technology (Neuroscience Associates).

Campbell-Switzer silver stain. A detailed protocol for this staining can be found on the Neuroscience Associate website (https://www.neuroscienceassociates.com/reference/papers/alzheimers-disease-pathology-silver-stain/). In particular, we have performed a semi-quantification of the Campbell-Switzer silver staining in the frontal, cingulate, entorhinal cortices, and hippocampus as this model develops extensive Aβ pathology and/or affected

significantly in these regions in this animal model.[2,17] Considering the limited number of animals at the end of the study (Tg-SAL = 2, Tg-ABP = 8), the amount of the Campbell-Switzer silver staining was quantified across subjects in each group as the percentage of the area of Campbell-Switzer silver staining in each region per slide (each data point represents the area of the Campbell-Switzer silver staining/the total area of each slide across subjects in each group).

Perls/DAB stain. For staining of ferric iron in tissue, every twelfth section (an interval of 480 μ) was stained free-floating. The sections were rinsed in dH$_2$O then placed in a freshly prepared (1:1) 2% HCL and 2% Potassium Ferrocyanide solution for 30 minutes at room temperature. The sections were again rinsed, then treated with a DAB solution (0.05% diaminobenzidine and 0.011% hydrogen peroxide) to amplify Perl's reaction product. Following further rinses, the sections were mounted on gelatin-coated glass slides, then air-dried. The mounted slides were then counterstained with a light Thionine Nissl counterstain.

Light thionine nissl counterstain. The mounted Perl's/DAB stained slides were dehydrated through alcohols. The slides were then rehydrated and stained in a Thionine solution made in an acetate buffer: pH4.5. Following deionized water rinses, the slides were cleared in xylene and coverslipped with Permount (Fisher Scientific, Pittsburgh PA).

Statistical analysis

All animals were randomly selected into Tg-SAL and Tg-ABP with age (21 months of age at baseline) and sex- and weight-matched. CSF NFL data were log-transformed to fit normality. When comparing between groups, the number of data points in each group is identified as Group1 vs Group2, while the number of data points from each sex is identified as M/F for males and females in all analyses, respectively. All statistical analyses were performed using parametric tests except for pharmacokinetic modelling following the Shapiro-Wilk normality test.

For statistical analyses, we have tested the pharmacokinetics of KG207-M in plasma and CSF based on nonlinear pharmacokinetics models (parameter estimates not shown) to evaluate the relationship between the central and peripheral compartments. To assess the longitudinal Aβ progression using PET imaging, we included the animals from our previous cohort data from 9-16 months to generate a population-based longitudinal Aβ progression model. We added a cohort term to adjust for its variability. We applied a linear mixed-effect model with a random intercept in the

Tg-ABP group alone to evaluate the target engagement: $[^{18}F]$AZD4694 $BP_{ND} \sim Age + Sex + Weight + (1|subject)$. Furthermore, we introduced an interaction term when using the whole dataset to directly assess the KG207-M effect between the groups where KG207-M was a binary variable representing 0 as animals without KG207-M treatment and 1 as Tg-ABP: $[^{18}F]$AZD4694 $BP_{ND} \sim Age*KG207\text{-}M + Age + KG207\text{-}M + Sex + Weight + cohort + (1|subject)$. The same interaction model was applied at the voxel level. Furthermore, we have examined the percentage of area Campbell-Switzer silver staining in frontal, cingulate, entorhinal cortices, and hippocampus based on an ANOVA including an interaction term between the percentage of area stained and different regions. Considering the primary objective of the study, we have applied a multiple comparisons correction using False Discovery Rate based on the number of regions. Similarly, we conducted a linear mixed-effect model using CSF $A\beta_{42/40}$ and CSF NFL_{log} with a random intercept and adjusted for sex and weight: CSF $A\beta_{42/40}$ ratio $\sim Age + Sex + Weight + (1|subject)$ or CSF $NFL_{log} \sim Age + Sex + Weight + (1|subject)$. Moreover, we evaluated the change in CSF $A\beta_{42/40}$ ratio and NFL_{log} between the last sample collected before the treatment (19-month sample) and after the treatment using a linear mixed-effect model in each group. In addition, a two-sided paired t-test was performed to compare the measured CSF $A\beta_{42/40}$ ratio and CSF NFL_{log} concentrations to the predicted levels based on the natural progression in the population-based model in two months following the treatment. Also, the longitudinal analysis in rs-fMRI and hippocampal volume were analyzed based on the following models: z-maps $\sim Age + Sex + Weight + (1|subject)$ and hippocampal volume $\sim Age + Sex + Weight + (1|subject)$, respectively, in each group. Last, a two-sided unpaired t-test was performed to compare the susceptibility MRI contrast signal between the groups at follow-up for any evidence of ARIA-H. All statistical analyses were performed using R 3.6.3, Prism7, and VoxelStats, while ImageJ 1.52a was used for the Campbell-Switzer silver staining.[21] All voxel-wise analyses were corrected for multiple comparisons using the Random Field Theory (RFT) method for an adjusted threshold of $p < 0.05$. This experiment has been conducted and reported following the ARRIVE guidelines 2.0.[22]

Results

FC5-mFC2a-ABP (KG207-M) fusion protein

The ABP fusion protein is schematically represented in Figure 2. FC5 is a single-domain camelid antibody that
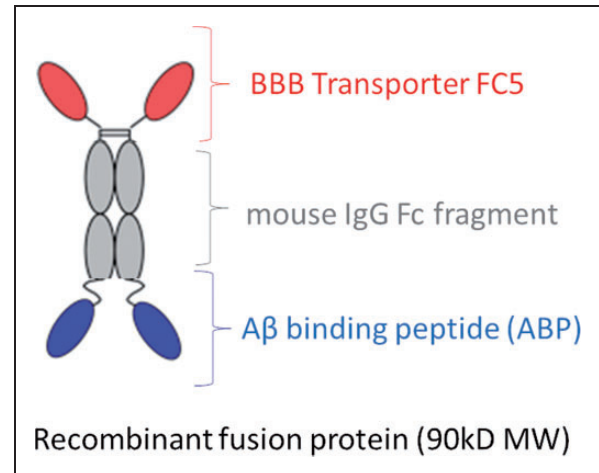

Figure 2. This is a schematic representation of KG207-M. The FC5 segment is in red, ABP is in blue, and the mouse IgG Fc fragment is in grey.

crosses BBB via receptor-mediated transcytosis. Fc fragment derived from mouse IgG2a increases the serum half-life. ABP is derived from human pericentriolar material 1 (PCM-1) that selectively binds to $A\beta_{42}$ oligomers at nM concentrations.[16] This fusion protein was successfully expressed and produced in a stable pool of CHO cells and purified using Protein A affinity column.

CSF appearance of peripherally administered KG207-M

KG207-M treatment followed the regimen as described in the Study Design in the Methods section (Figure 1). It was initiated in Tg rats at the age of 22.5 months and consisted of a total of five injections (initial loading dose of 30 mg/Kg/iv and subsequent 15 mg/Kg/iv every week for four weeks via tail vein) in the treatment group, while the control group received saline. The CSF and plasma samples were serially collected following KG207-M or saline administration at the indicated time intervals in the subsequent days (Day 1–7) to characterize serum PK and CSF exposure to the fusion protein.

As presented in Figure 3(a), observed (filled circles) and simulated curves (solid line) derived from a 2-compartment pharmacokinetic model (parameter estimates not shown) depict the average KG207-M plasma concentration fluctuations during the course of the study (M/F = 17/36). In addition, from an empirical pharmacokinetic model linking KG207-M plasma to CSF concentration dynamics, approximate fluctuations of KG207-M CSF concentration (solid line) vs observed concentrations (filled circles) are represented (M/F = 15/8) (b). Based on the structure of an
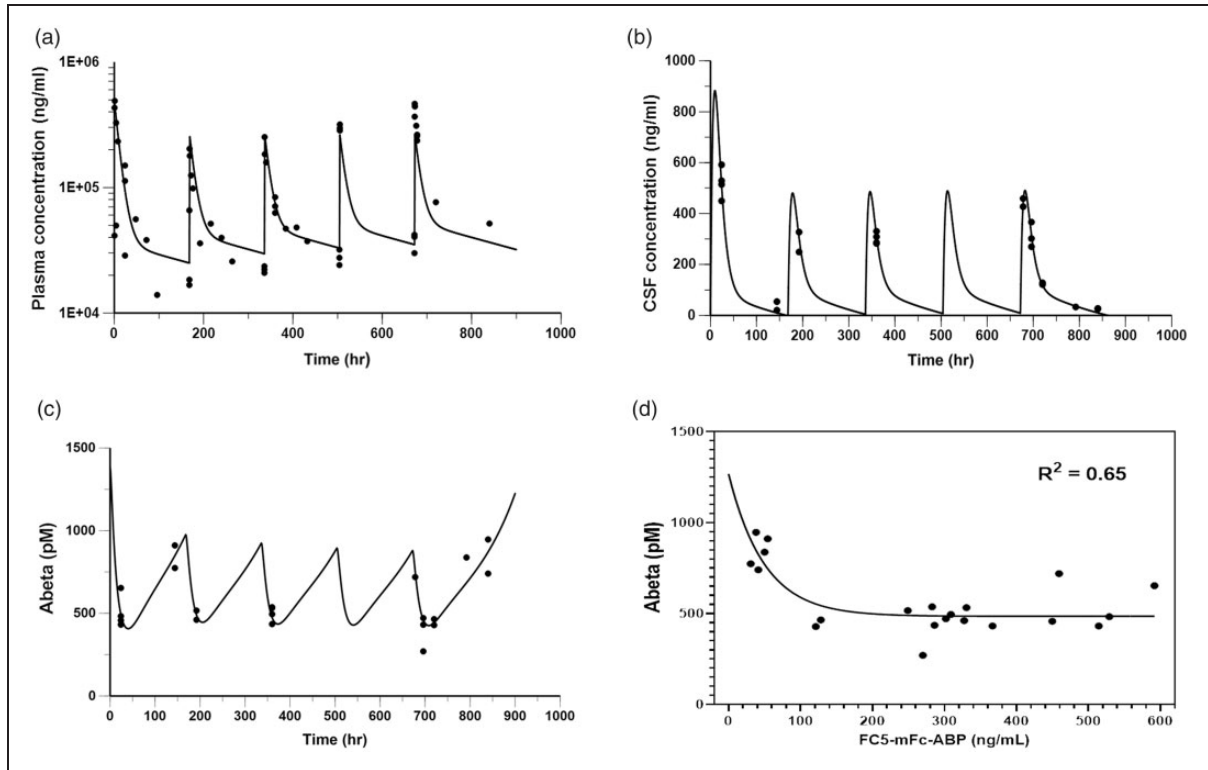
Figure 3. (a, b & c) Observed (filled circles) and simulated (solid line) KG207-M (a & b) or total Aβ. (Aβ_{total}) (c). The KG207-M concentration in plasma (a) or CSF (b & c) vs time following administration of 30 mg/kg/iv bolus followed by four 15 mg/kg/iv bolus doses every 7 days for 28 days to Tg-ABP rats are shown. (d) Aβ_{total} concentration vs KG207-M concentration in CSF.

indirect-response PK/PD model where KG207-M stimulates the clearance of Aβ_{total}, a simulated profile of Aβ_{total} is presented in panel (c) in Figure 3 (M/F = 15/8). The model supports an inverse relation between CSF KG207-M concentrations and CSF Aβ_{total} concentrations (M/F = 15/8). Panel (d) in Figure 3 indicates that the clearance of Aβ_{total} CSF reaches an asymptote when CSF KG207-M reaches 200 ng/mL. The simulations presented in panel (b) in Figure 3 depicted the maintenance of KG207-M CSF concentration above 200 ng/ml for approximately 20% of the dosing interval.

KG207-M reduces Aβ load in the brain and CSF

The natural progression of Aβ accumulation in Tg rats was demonstrated via longitudinal PET [^{18}F]AZD4694 quantification (BP$_{\text{ND}}$). The global Aβ load significantly increased in Tg rats from 9 to 24 months of age (population main effect model: M/F = 14/13, t(21) = 2.474, p = 0.0349) (Figure 4(a)). Following the KG207-M treatment initiated at 21 months of age, [^{18}F]AZD4694 BP$_{\text{ND}}$ substantially decreased in the Tg-ABP at 24 months (main effect model: M/F = 12/4, t(7.4) = −2.657, p = 0.03112), showing KG207-M target engagement. When we compare the Aβ pathology progression

between the Tg-SAL and Tg-ABP, we found that KG207-M significantly altered the Aβ pathology progression in the Tg-ABP group adjusted for sex, weight, and cohort variability (interaction model: cohort 1 and Tg-SAL vs Tg-ABP = 21 vs 16, M/F = 16/21, t (17.3) = −3.321, p = 0.00397) (Figure 4(a)).

We also evaluated the effects of KG207-M on the CSF A$\beta_{42/40}$ ratio in Tg following the KG207-M treatment. The CSF was collected from 10 to 19 months old prior to the KG207-M treatment to characterize the natural longitudinal CSF A$\beta_{42/40}$ ratio progression model in Tg. There was a progressive and significant decline in the CSF A$\beta_{42/40}$ ratio adjusted for sex and weight (M/F = 40/84, t(114.4) = −2.971, p = 0.00362) (Figure 4(b)). However, there was a significant increase in the CSF A$\beta_{42/40}$ measurements from 0.531 at 19 months old to 0.63 following two months after the KG207-M treatment in the Tg-ABP group (main effect model: M/F = 16/6, t(15.34) = 2.4, p = 0.03), while the Tg-SAL group showed a significant decline from 0.50 at 19 months to mean of 0.43 at 25 and 26 months (main effect model: M/F = 4/3, t(7) = −6.32, p = 0.0004). To note, the Tg-ABP group seemed to carry slightly more Aβ pathology, which enriched the effect of the treatment, relative to Tg-SAL, but this was not statistically different. Furthermore, when we
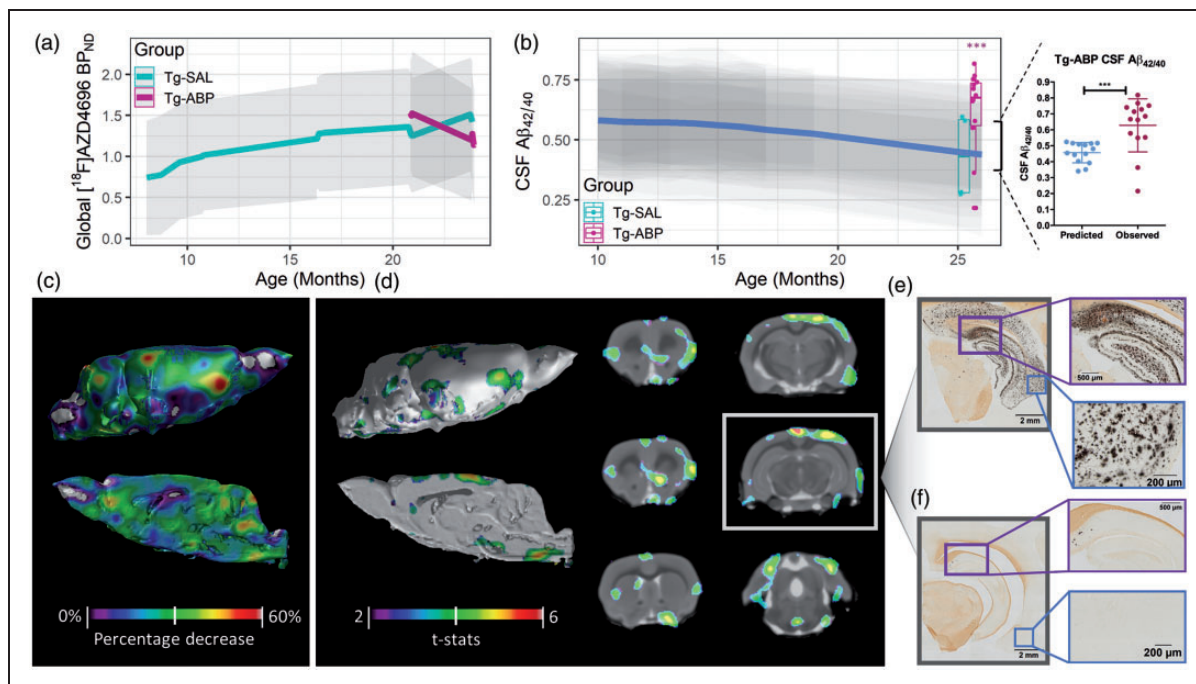
Figure 4. The gray shadow represents the 95% confidence intervals of models in (a and b). (a) The linear mixed-effect model of global [^{18}F]AZD4694 BP$_{ND}$ showed a significant increase in Tg from 10 to 24 months old (solid green line; t(21) = 2.437, p = 0.0238; adjusted for sex, weight, and cohort variability) but a significant decline in Tg-ABP between 21 to 24 months old (solid red; t(7.4) = − 2.657, p = 0.03112; adjusted for sex and weight). The interaction between treatment and disease progression showed that KG207-M significantly modified global [^{18}F]AZD4694 BP$_{ND}$ (cohort 1 and Tg-SAL vs Tg-ABP = 21 vs 16, M/F = 16/21, t(17.3) = −3.321, p = 0.00397; adjusted for sex, weight, and cohort variability). (b) The linear mixed-effect model showed a significant decline in CSF A$\beta_{42/40}$ ratio in Tg rat model from 10 to 19 months old (solid blue; t(114.4) = −2.971, p = 0.00362, adjusted for sex and weight). A box whisker plot based on Tukey method represented a paired t-test, which revealed that CSF A$\beta_{42/40}$ ratio increased (solid red; t (13) = 4.373, p = 0.0008) in Tg-ABP animals as compared with a population-based prediction by the model while no differences were found in Tg-SAL (t(3) = 0.4869, p = 0.6597). (c) A voxel-wise effect size map showed up to 47% decline in [^{18}F]AZD4694 BP$_{ND}$ prefrontal region (baseline-follow-up/baseline). (d) A voxel-wise linear mixed-effect model analysis showed a significant [^{18}F]AZD4694 BP$_{ND}$ clearance in the prefrontal cortex, cingulate cortex, entorhinal cortex, hippocampus, and basal forebrain in Tg-ABP compared to Tg-SAL (cohort 1 and Tg-SAL vs Tg-ABP = 21 vs 16, M/F = 16/21, adjusted for sex, weight, and cohort variability). The interaction term was corrected for multiple comparisons based on RFT at p < 0.05. (e, f) Campbell-Switzer silver staining displayed widespread Aβ plaques throughout the cortical regions in Tg-SAL animals while relatively few plaques were seen in Tg-ABP brains collected at 26.7 months old (Tg-SAL vs Tg-ABP = 2 vs 8, M/F = 7/5, t(24) > 4, p < 0.001). Here, one brain image from each group was included but comparable results were seen in all animals from each group.

compared the CSF A$\beta_{42/40}$ measurements following two months after the KG207-M treatment compared to the non-treated condition predicted by the longitudinal model, we found a significant increase showing rectification of the CSF A$\beta_{42/40}$ profile in the Tg-ABP (a paired t-test: M/F = 10/4, t(13) = 4.35, p = 0.0008) (Figure 4(b)). On the other hand, Tg-SAL did not show any difference compared to the predicted longitudinal model (Figure 4(b)). The monthly CSF Aβ_{42} and Aβ_{40} concentrations are summarized in Supplemental Table 1.

Then, we investigated the disease-modifying therapeutic effects of KG207-M using voxel-wise analyses and revealed up to 47% and 33% decline in [^{18}F] AZD4694 BP$_{ND}$ in the prefrontal cortex and nucleus accumbens, respectively, after the KG207-M treatment

(Figure 4(c)). Moreover, the reductions in the [^{18}F] AZD4694 BP$_{ND}$ were statistically significant in the prefrontal cortex, cingulate cortex, entorhinal cortex, associative cortex, retrosplenial cortex, nucleus accumbens, and hippocampus (interaction model: cohort 1 and Tg-SAL vs Tg-ABP = 21 vs 16, M/F = 16/21, t = 2-6). (Figure 4(d)). It is worth noting that these brain regions play important roles in rat cognitive functions and are vulnerable to Aβ pathology in this model displaying extensive Aβ plaques.[2,17] A more comprehensive view of the voxel-wise results can be found in Supplemental Figure 1.

The imaging analyses were supported by the postmortem histology using Campbell-Switzer silver staining. We observed extensive Aβ plaques in the frontal cortex (15%), cingulate cortex (13%), entorhinal cortex

(18.4%), and hippocampus (24%) in Tg-SAL brains (Figure 4(e)). However, there was minimal to no staining in Tg-ABP brains (<0.01% in all regions). Based on an ANOVA test, Tg-ABP showed a significantly less percentage of the Campbell-Switzer silver staining in all regions (Tg-SAL vs Tg-ABP = 2 vs 8, M/F = 7/3, t (24) > 4, p < 0.001) following a multiple comparisons correction based on the number of regions tested, supporting the clearance and prevention of Aβ plaque formation (Figure 4(f) and Supplemental Figure 2).

KG207-M rescues neuronal injury biomarkers

In addition to the longitudinal CSF $A\beta_{42/40}$ ratio progression, CSF NFL_{log} concentrations were analyzed as a biomarker of neuronal injury over 10-19 months of age in the McGill-R-Thy1-APP rat model prior to administration of KG207-M. Recent reports showed increased concentrations of CSF NFL in AD and other neurodegenerative diseases and reduced CSF NFL concentrations following beta-secretase 1 (BACE-1) inhibitor treatment in APPPS1 mice, suggesting that CSF NFL is a sensitive neuronal injury biomarker.[23–25] A progressive and significant increase in CSF NFL_{log} concentrations was observed in Tg rats over 10-19 months of age (M/F = 54/25, t(67.6) = 4.65, p < 0.0001; adjusted for sex and weight), and it continued to increase significantly in the Tg-SAL group when we compared from the beginning of the treatment (32958 pg/mL) and the post-treatment samples (49190.5 pg/mL) (main effect model: M/F = 4/3, t(7) = 4.47, p = 0.003) (Figure 5(a)). However, the Tg-ABP group showed no significant increase in CSF NFL_{log} concentration between the beginning of the treatment (39405 pg/mL) and the post-treatment samples (44375.5 pg/mL). Rather, there was a significant reduction in CSF NFL_{log} concentration following two months after KG207-M treatment compared to the
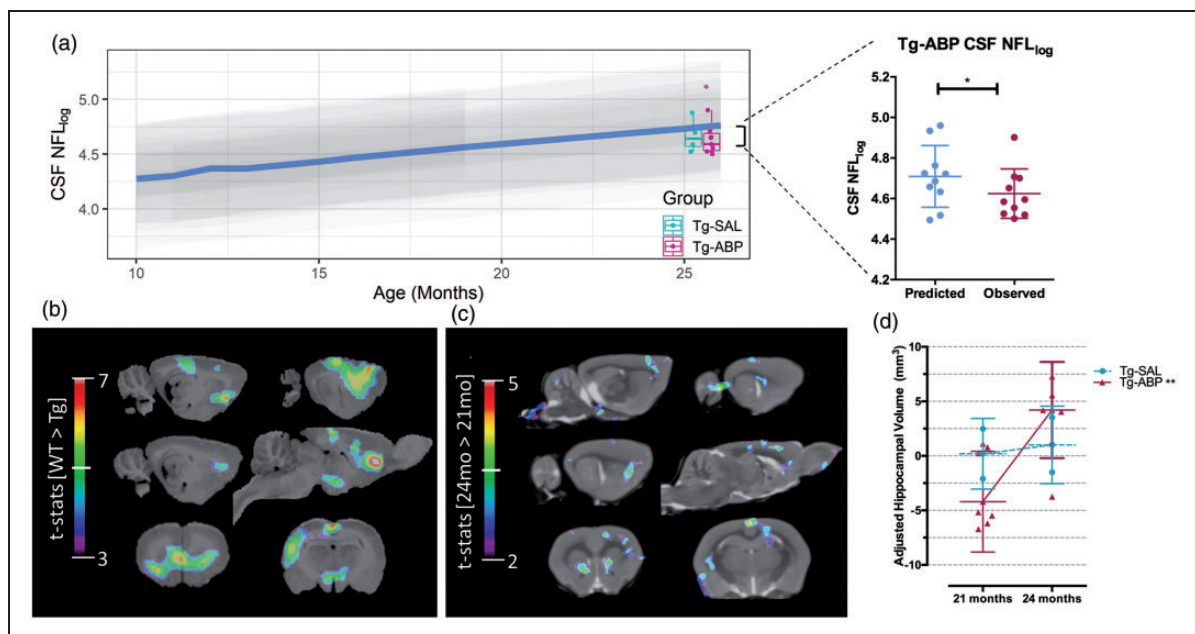
Figure 5. (a) The gray shadow represents the 95% confidence intervals of the model per subject. The linear mixed-effect model showed a significant increase in CSF NFL_{log} concentrations, represented after log transformation, in the Tg rat model from 10 to 19 months old (solid blue; t(67.6) = 4.819, p < 0.0001; adjusted for sex and weight). A box whisker plot based on Tukey method represented a paired t-test, which revealed that CSF NFL_{log} concentrations decreased (solid red; t(9) = 2.6286, p = 0.0481) in Tg-ABP as compared to a population-based prediction by the model while Tg-SAL showed no difference (t(3) = 1.208, p = 0.3137). (b) The figure represents a significant group contrast in resting-state blood-oxygen-level-dependent (BOLD) signal from cingulate to the rest of the brain between WT (n = 8) and McGill-R-Thy1-APP (n = 8) at 16-19 months. The voxel-wise linear mixed-effect analysis showed a significant reduction in resting-state cingulate connectivity in the basal forebrain, parietal associative cortex, and hippocampus in Tg (reproduced from Parent et al.[17]) The result images were adjusted for multiple comparisons based on RFT at p < 0.05. (c) The figure represents a significant contrast in the resting-state BOLD signal from cingulate to the brain in Tg-ABP (n = 9) following KG207-M treatment compared to baseline at 21 months of age. The voxel-wise linear mixed-effect analysis showed a significant increase in resting-state cingulate connectivity in the basal forebrain, parietal associative cortex, and hippocampus when the network is compared before and after KG207-M treatment. The result images were adjusted for multiple comparisons based on RFT at p < 0.05. (d) The adjusted hippocampal volume in Tg-SAL and Tg-ABP before and after KG207-M treatment are displayed as mean ± standard deviation. The linear mixed-effect analysis revealed a significant increase in hippocampal volume in Tg-ABP (t(7) = 3.554, p = 0.00397; adjusted for sex and weight), however, there was no significant hippocampal volume change in Tg-SAL (t(1) = 0.1694, p = 0.8932).

non-treated condition predicted by the longitudinal model suggesting a reduction in neuronal injury (paired t-test: $M/F = 6/4$, $t(9) = 2.28$, $p = 0.0487$) (Figure 5(a)). The monthly CSF NFL concentrations are summarized in Supplemental Table 2.

Furthermore, using the same Tg model and techniques, our group has recently reported a decline in cingulate resting-state connectivity (Figure 5(b)) as well as hippocampal volume in the McGill-R-Thy1-APP Tg model compared to wild type.[17] Here, Tg-ABP cingulate to brain connectivity was increased after five weeks of KG207-M treatment while Tg-SAL showed no change. Tg-ABP showed greater cingulate connectivity with the orbitofrontal cortex, somatosensory cortex, parietal association cortex, basal medial amygdaloid nucleus, left posterior ventral hippocampus, striatum, and thalamus (main effect model: $M/F = 12/4$, $t = 2–5$) (Figure 5(c)). A more comprehensive view of the voxel-wise results can be found in Supplemental Figure 3. In addition, Tg-ABP showed a substantial increase in hippocampal volume after the treatment while Tg-SAL did not change in their hippocampal volume adjusted for sex and weight (Tg-ABP paired t-test; $M/F = 12/4$, $t(7) = 3.554$, $p = 0.00397$) (Figure 5(d)).

No evidence of microhemorrhage

To examine any possible ARIA-H, we conducted a susceptibility MRI scan following the treatment. The images were visually assessed first to see possible ARIA-H. Asymmetric susceptibility signals were the primary interest as the vascular structures displayed symmetry (Figure 6(a)). In conjunction, the susceptibility signal was binarized to represent either vasculature, ventricles, or ARIA-H. There was no difference in susceptibility signal volume between Tg-SAL and Tg-ABP (unpaired t-test; Tg-SAL vs Tg-ABP $= 3$ vs 9, $M/F = 7/5$, $t(2.59) = 0.455$, $p = 0.685$) (Figure 6(c)). This was confirmed by post-mortem histology staining with Perls/DAB (Figure 6(b)).

Discussion

In summary, our study demonstrated the pharmacokinetics, safety, and disease-modifying effects of KG207-M that incorporates a BBB transporter and an $A\beta_{42}$ oligomer targeting peptide. Effectively, KG207-M showed sufficient brain penetrance to reduce $A\beta_{42}$ aggregates. This was demonstrated by the acute decline in CSF $A\beta_{total}$ concentration when KG207-M was at its
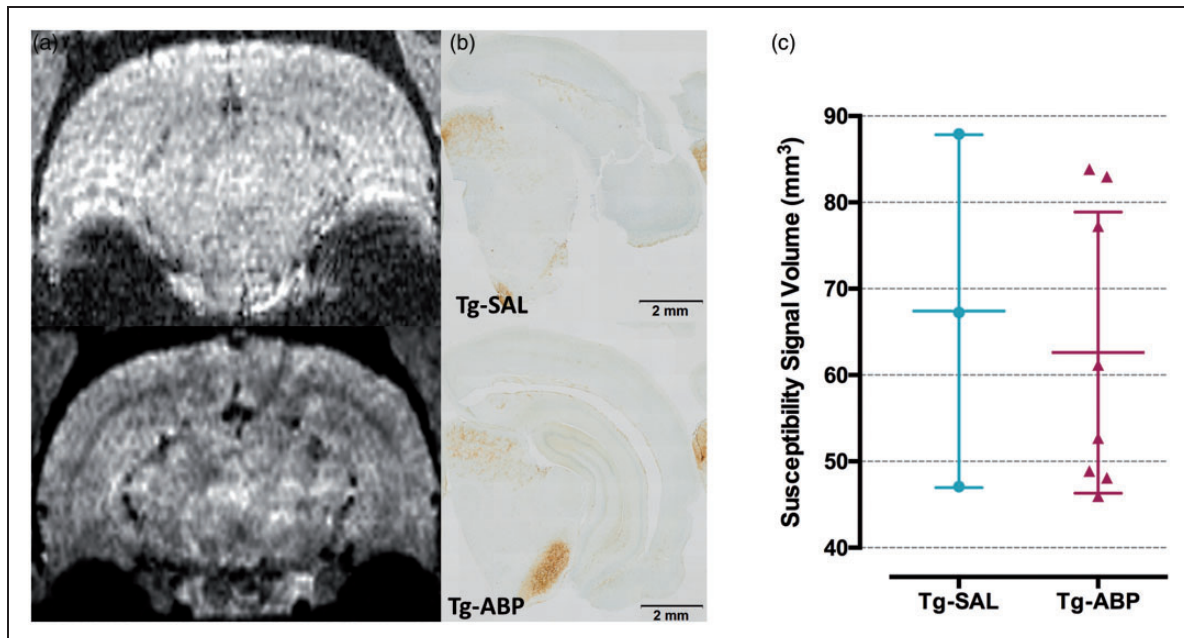
Figure 6. (a) The susceptibility MRI in the coronal view of Tg-SAL in the upper corner image and Tg-ABP in the lower corner. Both images do not show any evidence of ARIA-H. (b) Histological staining using Perls/DAB of the same animals in the corresponding section from the susceptibility images are shown. These sections were taken adjacent to the previous Campbell-Switzer silver staining section. In both Tg-SAL and Tg-ABP, there is no evidence of ARIA-H. (c) Susceptibility signal contrast was converted into volume and displayed in mean ± standard deviation in Tg-SAL (n = 3) and Tg-ABP (n = 9). The contrast signal implies that there is a deposit of iron (ARIA-H), vasculatures, or ventricles. There was no significant difference in susceptibility signal contrast volume between Tg-SAL and Tg-ABP after five weeks of KG207-M treatment (unpaired t-test; Tg-SAL vs Tg-ABP = 3 vs 9, M/F = 7/5, t(2.59) = 0.455, p = 0.685).

maximum concentration in CSF and by the subsequent reduction of PET [^{18}F]AZD4694 uptake. The *in vivo* results were validated by the semi-quantitative observation conducted in the post-mortem tissues of the Tg-ABP animals using Campbell-Switzer silver staining. In addition, KG207-M therapeutic efficacy in reducing downstream effects of Aβ accumulation was demonstrated by the substantial post-therapeutic recovery of CSF A$\beta_{42/40}$ ratios and CSF NFL$_{log}$ concentrations, increased hippocampal volume, and rectification of rs-fMRI cingulate to brain connectivity. Last, the absence of ARIA-H supports a safe profile of the doses administered to these animals.

Previously FC5-Fc has been shown to reach peak CSF/serum level ($\geq$ 1%) between 24 and 48 hours post tail vein injection, which is much higher than the conventional antibodies.[26,27] Based on the results of recent anti-amyloid therapy clinical trials, one may argue that the BBB delivery could impact therapeutic efficacy.[6,8,11] Maintaining the CSF levels of KG207-M at an effective dose (200 ng/ml) in this prospective study sufficiently reduced the Aβ loads in Tg-ABP animals. Importantly, our study supports the notion that KG207-M delivery using the humanized FC5-Fc nanobody via receptor-mediated transcytosis, which is conserved between rodents and humans, would be sufficient to transport the drug and modify Aβ pathology in human clinical trials.[14]

With abundant evidence suggesting soluble oligomers being the most toxic form of Aβ, the preferential binding to the aggregated Aβ by KG207-M suggests that it can selectively target Aβ_{42} oligomers in the CNS.[15,16,28–30] Despite the lack of direct measures of target engagement of Aβ_{42} oligomers non-invasively, the decline in [^{18}F]AZD4694 uptake and rectification of CSF A$\beta_{42/40}$ ratio in the post-treatment measurement in Tg-ABP constitute remarkable proof of concept of the KG207-M intervention. The reduced brain Aβ loads reported here are likely to reflect Aβ oligomer clearance, under the assumption of dynamic equilibrium among Aβ species in these animals.[30,31] As such, one can expect that Aβ_{42} oligomer clearance evoked by KG207-M would shift this dynamic equilibrium towards reducing the amount of Aβ plaques, and consequently reducing the [^{18}F]AZD4694 uptake. A similar observation made in the PRIME study showed a reduction of PET-[^{18}F]AV45 uptake following aducanumab treatment, an intervention that targets either soluble oligomers or insoluble fibrils.[8] Indeed, after the cessation of KG207-M administration, the levels of CSF A$\beta_{42/40}$ were rectified until the animals were sacrificed for histological examination.

It has been challenging to predict the effects of therapeutic interventions on human imaging biomarkers based solely on *in vitro* histopathological observations in animals. In addition, the cross-sectional nature of *in vitro* observations limits the prediction in the post-therapy Aβ levels compared to its pre-dosing levels.[32] Although solanezumab and bapineuzumab were successful in the preclinical stage of drug development, both therapeutic candidates failed to meet the clinical primary outcome as well as reducing Aβ load with PET in their phase 3 studies.[6,7] In this study, we attempted to reduce the gap between pre-clinical and clinical studies through a highly translational platform by incorporating a longitudinal study design with fluid and imaging biomarkers to monitor KG207-M therapeutic effects in the McGill-R-Thy1-APP rat model. These innovations offer unprecedented metrics regarding the true effect sizes of KG207-M on engaging the molecular targets, on rectifying neuronal injury based on structural and functional biomarkers, as well as providing a safety profile via the same biomarkers used in clinical trials.

This platform capitalizes on the properties of the McGill-R-Thy1-APP rat model, which has been previously characterized based on the *in vivo* biomarker platform.[17,33] The McGill-R-Thy1-APP rat model progressively develops Aβ pathology, indicated by the significant increase in the [^{18}F]AZD4694 PET and decline in the CSF A$\beta_{42/40}$ ratio, at a similar rate as AD patients and recapitulates AD biomarker abnormalities.[17,33] For example, the McGill-R-Thy1-APP rat model has an increased CSF NFL concentration, reduction in hippocampal volume, cingulate connectivity, and CSF A$\beta_{42/40}$ ratio, which have been shown to be sensitive biomarkers for AD pathological progression and disease severity, ultimately leading to memory impairment.[13,17,24,33–39] In addition to the disease-modifying effect, five weeks of KG207-M treatment ameliorates the hippocampal volume, cingulate connectivity, and CSF A$\beta_{42/40}$ ratio and CSF NFL concentrations, among which CSF NFL and resting-state connectivity dysfunction were reported to be due to Aβ oligomers in this Tg rat model.[17,33] It is important to interpret the volumetric changes observed based on MRI in the animals with caution as such changes do not necessarily reflect neurogenesis. Rather, collective evidence suggests synaptic recovery through the dendritic growth and/or synaptic remodelling as the McGill-R-Thy1-APP rats have shown a decline in volumetric changes without significant cell death.[17,33,40] Nevertheless, to the best of our knowledge, this is the first study to show directly the therapeutic target engagement, efficacy, and safety using multiparametric clinical biomarkers such as CSF, PET, and MRI in a preclinical *in vivo* longitudinal study.

It is imperative to recognize some limitations of the present study. There were no prior data to precisely estimate an effect size for ARIA-H as this study was

the first *in vivo* characterization of KG207-M. While no increase in microhemorrhages was observed in the present study, a separate study should be conducted to more fully assess the ARIA potential of KG207-M — possibly in an animal model with known microhemorrhage susceptibility and with a positive control microhemorrhage-inducing antibody. Moreover, currently, there is no established method to accurately quantify the changes in $A\beta_{42}$ oligomers levels directly *in vivo*. As such, different methods of $A\beta$ quantifications were used as a surrogate for $A\beta_{42}$ oligomers clearance. Also, the McGill-R-Thy1-APP rat model develops $A\beta$ pathology progressively at levels comparable to human patients. However, it lacks tau pathology that is present invariably in AD patients leading to a lack of substantial cell death in this model.[2,17,40] Previous studies have reported that neurofibrillary tangles (NFT) show a greater correlation with structure and memory declines as NFT are in closer proximity to the downstream AD pathological processes.[41] As such, our study did not evaluate cognitive changes following the treatment in the McGill-R-Thy1-APP rat model. Albeit the primary objective of the study was to characterize the target engagement, assessment of cognitive improvement will be critical to demonstrate therapeutic value, and this will be pursued in a subsequent study to address this limitation in the current study. While we report improvement in CSF NFL, cingulate connectivity, and hippocampal volume by targeting $A\beta$ pathology, one should be cautious in expecting full translation in the therapeutic efficacy on neuronal injury biomarkers in AD patients. Perhaps, the discrepancies reported insofar between preclinical and clinical trials regarding cognitive improvement may lie in this aspect.

With the evidence presented here based on our *in vivo* longitudinal translational biomarker platform, KG207-M holds great potential as disease-modifying therapy. By constructing ABP to selectively target more toxic forms of $A\beta_{42}$, KG207-M does not only alter $A\beta$ pathological progression but also rescues the typical biomarker changes that are reported in the McGill-R-Thy1-APP rat model. This is a unique effort to evaluate the disease-modifying therapeutic effects and safety in a preclinical study. Consequently, we propose that this will increase the chance of translating the findings into clinical trials.

Declaration of conflicting interests

The author(s) declared the following potential conflicts of interest with respect to the research, authorship, and/or publication of this article: Dr. Blennow has served as a consultant or at advisory boards for Alzheon, BioArctic, Biogen, Eli Lilly, Fujirebio Europe, IBL International, Merck, Novartis, Pfizer, and Roche Diagnostics, all unrelated to the present study, and is a co-founder of Brain Biomarker Solutions in Gothenburg AB, a GU Venture-based platform company at the University of Gothenburg.

Authors' contributions

M.S.K., M.S., N.Y., D.S., B.C., and P.R-N. designed the study. M.S.K., M.S., A.A.A., A.M., and M.M.C. collected the *in vivo* imaging data. M.S.K. and J.O. analyzed the *in vivo* imaging data. M.S.K., A.A.A, and K.Q.S. collected in vitro rat brain tissues. M.S.K. analyzed the in vitro microhemorrhage data. A.S., K.B., H.Z., A.H., and B.C. analyzed the CSF fluid data. A.H. and B.C. analyzed plasma data. M.S.K., S.M., J.O., K.R., B.C., and P.R-N. conducted statistical analyses. M.S.K., T.A.P., A.L.B., D.L.C., J-P.S., M.M.C., A.M., A.S., K.B., H.Z., G.M., A.C.C., S.G., M.W., E.L., A.H., K.R., D.S., B.C., and P.R-N., wrote and revised the manuscript.

ORCID iDs

Min Su Kang https://orcid.org/0000-0003-0745-6222
Julie Ottoy https://orcid.org/0000-0002-9879-7497
Pedro Rosa-Neto https://orcid.org/0000-0001-9116-1376

Supplemental material

Supplemental material for this article is available online.

References

1. Hardy J and Selkoe DJ. The amyloid hypothesis of Alzheimer's disease; progress and problems on the road to therapeutics. *Science* 2002; 297: 353–356.
2. Leon WC, Canneva F, Partridge V, et al. A novel transgenic rat model with a full Alzheimer's-like amyloid pathology displays pre-plaque intracellular

amyloid-beta-associated cognitive impairment. *J Alzheimers Dis* 2010; 20: 113–126.

3. O'Brien RJ and Wong PC. Amyloid precursor protein processing and Alzheimer's disease. *Annu Rev Neurosci* 2011; 34: 185–204.

4. Kadowaki H, Nishitoh H, Urano F, et al. Amyloid beta induces neuronal cell death through ROS-mediated ASK1 activation. *Cell Death Differ* 2005; 12: 19–24.

5. Choi SH, Kim YH, Hebisch M, et al. A three-dimensional human neural cell culture model of Alzheimer's disease. *Nature* 2014; 515: 274–278.

6. Doody RS, Thomas RG, Farlow M, et al.; Solanezumab Study Group. Phase 3 trials of solanezumab for mild-to-moderate Alzheimer's disease. *N Engl J Med* 2014; 370: 311–321.

7. Salloway S, Sperling R, Fox NC, et al.; Bapineuzumab 301 and 302 Clinical Trial Investigators. Two phase 3 trials of bapineuzumab in mild-to-moderate Alzheimer's disease. *N Engl J Med* 2014; 370: 322–333.

8. Sevigny J, Chiao P, Bussiere T, et al. The antibody aducanumab reduces abeta plaques in Alzheimer's disease. *Nature* 2016; 537: 50–56.

9. Scholl M, Lockhart SN, Schonhaut DR, et al. PET imaging of tau deposition in the aging human brain. *Neuron* 2016; 89: 971–982.

10. Hardy J and De Strooper B. Alzheimer's disease: where next for anti-amyloid therapies? *Brain* 2017; 140: 853–855.

11. Selkoe DJ and Hardy J. The amyloid hypothesis of Alzheimer's disease at 25 years. *EMBO Mol Med* 2016; 8: 595–608.

12. Rowe CC, Pejoska S, Mulligan RS, et al. Head-to-head comparison of 11C-PiB and 18F-AZD4694 (NAV4694) for beta-amyloid imaging in aging and dementia. *J Nucl Med* 2013; 54: 880–886.

13. Janelidze S, Zetterberg H, Mattsson N, et al.; Swedish BioFINDER Study Group. CSF Abeta42/Abeta40 and Abeta42/Abeta38 ratios: better diagnostic markers of Alzheimer disease. *Ann Clin Transl Neurol* 2016; 3: 154–165.

14. Abulrob A, Zhang J, Tanha J, et al. Single domain antibodies as blood–brain barrier delivery vectors. *Int Congr Series* 2005; 1277: 212–223.

15. Chakravarthy B, Menard M, Brown L, et al. A synthetic peptide corresponding to a region of the human pericentriolar material 1 (PCM-1) protein binds beta-amyloid (Abeta1-42) oligomers. *J Neurochem* 2013; 126: 415–424.

16. Chakravarthy B, Ito S, Atkinson T, et al. Evidence that a synthetic amyloid-ss oligomer-binding peptide (ABP) targets amyloid-ss deposits in transgenic mouse brain and human Alzheimer's disease brain. *Biochem Biophys Res Commun* 2014; 445: 656–660.

17. Parent MJ, Zimmer ER, Shin M, et al. Multimodal imaging in rat model recapitulates Alzheimer's disease biomarkers abnormalities. *J Neurosci* 2017; 37: 12263–12271.

18. Haqqani AS, Caram-Salas N, Ding W, et al. Multiplexed evaluation of serum and CSF pharmacokinetics of brain-targeting single-domain antibodies using a NanoLC-SRM-ILIS method. *Mol Pharmaceutics* 2013; 10: 1542–1556..

19. Friedel M, van Eede MC, Pipitone J, et al. Pydpiper: a flexible toolkit for constructing novel registration pipelines. *Front Neuroinform* 2014; 8: 67.

20. Rohrer JD, Woollacott IOC, Dick KM, et al. Serum neurofilament light chain protein is a measure of disease intensity in frontotemporal dementia. *Am Acad Neurol* 2016; 87: 1329–1336.

21. Mathotaarachchi S, Wang S, Shin M, et al. VoxelStats: a MATLAB package for multi-modal voxel-wise brain image analysis. *Front Neuroinform* 2016; 10: 20.

22. Percie Du Sert N, Hurst V, Ahluwalia A, et al. The ARRIVE guidelines 2.0: updated guidelines for reporting animal research. *J Cereb Blood Flow Metab* 2020; 40: 1769–1777.

23. Bacioglu M, Maia LF, Preische O, et al. Neurofilament light chain in blood and CSF as marker of disease progression in mouse models and in neurodegenerative diseases. *Neuron* 2016; 91: 56–66.

24. Zetterberg H, Skillback T, Mattsson N, et al.; for the Alzheimer's Disease Neuroimaging Initiative. Association of cerebrospinal fluid neurofilament light concentration with Alzheimer disease progression. *JAMA Neurol* 2016; 73: 60–67.

25. Scherling CS, Hall T, Berisha F, et al. Cerebrospinal fluid neurofilament concentration reflects disease severity in frontotemporal degeneration. *Ann Neurol* 2014; 75: 116–126.

26. Banks WA, Terrell B, Farr SA, et al. Passage of amyloid beta protein antibody across the blood-brain barrier in a mouse model of Alzheimer's disease. *Peptides* 2002; 23: 2223–2226.

27. Farrington GK, Caram-Salas N, Haqqani AS, et al. A novel platform for engineering blood-brain barrier-crossing bispecific biologics. *Faseb J* 2014; 28: 4764–4778.

28. Ahmed M, Davis J, Aucoin D, et al. Structural conversion of neurotoxic amyloid-beta(1-42) oligomers to fibrils. *Nat Struct Mol Biol* 2010; 17: 561–567.

29. Yang T, Li S, Xu H, et al. Large soluble oligomers of amyloid beta-protein from Alzheimer brain are far less neuroactive than the smaller oligomers to which they dissociate. *J Neurosci* 2017; 37: 152–163.

30. Mucke L and Selkoe DJ. Neurotoxicity of amyloid beta-protein: synaptic and network dysfunction. *Cold Spring Harb Perspect Med* 2012; 2: a006338–07.

31. DeMattos RB, Bales KR, Parsadanian M, et al. Plaque-associated disruption of CSF and plasma amyloid-beta (abeta) equilibrium in a mouse model of Alzheimer's disease. *J Neurochem* 2002; 81: 229–236.

32. Karran E and Hardy J. A critique of the drug discovery and phase 3 clinical programs targeting the amyloid hypothesis for Alzheimer disease. *Ann Neurol* 2014; 76: 185–205.

33. Kang MS, Aliaga AA, Shin M, et al. Amyloid-beta modulates the association between neurofilament light chain and brain atrophy in Alzheimer's disease. *Mol Psychiatry*. Epub ahead of print 26 June 2020. DOI: 10.1038/s41380-020-0818-1.

34. Dickerson BC and Wolk DA; Alzheimer's Disease Neuroimaging Initiative. Alzheimer's disease neuroimaging I. Biomarker-based prediction of progression in MCI: comparison of AD signature and hippocampal volume with spinal fluid amyloid-beta and tau. *Front Aging Neurosci* 2013; 5: 55–10.

35. Schuff N, Woerner N, Boreta L, et al.; Alzheimer's Disease Neuroimaging Initiative. MRI of hippocampal volume loss in early Alzheimer's disease in relation to ApoE genotype and biomarkers. *Brain* 2009; 132: 1067–1077.

36. Greicius MD, Srivastava G, Reiss AL, et al. Default-mode network activity distinguishes Alzheimer's disease from healthy aging; evidence from functional MRI. *Proc Natl Acad Sci USA* 2004; 101: 4637–4642.

37. Buckner RL, Snyder AZ, Shannon BJ, et al. Molecular, structural, and functional characterization of Alzheimer's disease: evidence for a relationship between default activity, amyloid, and memory. *J Neurosci* 2005; 25: 7709–7717.

38. Sheline YI and Raichle ME. Resting state functional connectivity in preclinical Alzheimer's disease. *Biol Psychiatry* 2013; 74: 340–347.

39. Blennow K. A review of fluid biomarkers for Alzheimer's disease: moving from CSF to blood. *Neurol Ther* 2017; 6: 15–24.

40. Heggland I, Storkaas IS, Soligard HT, et al. Stereological estimation of neuron number and plaque load in the hippocampal region of a transgenic rat model of Alzheimer's disease. *Eur J Neurosci* 2015; 41: 1245–1262.

41. Brier MR, Gordon B, Friedrichsen K, et al. Tau and Ab imaging, CSF measures, and cognition in Alzheimer's disease. *Sci Transl Med* 2016; 8: 338ra66.